RADARCLINOMETRY

ROBERT L. WILDEY

Branch of Astrogeology, U.S. Geological Survey and Department of Physics and Astronomy, Northern Arizona University, Flagstaff, Ariz., U.S.A.

(Received 27 September, 1985)

Abstract. A mathematical theory and a corresponding algorithm have been developed to derive topographic maps from radar images as photometric arrays. Thus, as radargrammetry is to photogrammetry, so radarclinometry is to photoclinometry. Photoclinometry is endowed with a fundamental indeterminacy principle even for terrain homogeneous in normal albedo. This arises from the fact that the geometric locus of orientations of the local surface normal that is consistent with a given reflected specific-intensity of radiation is more complicated than a fixed line in space. For a radar image, the locus is a cone whose half-angle is the incidence angle and whose axis contains the radar. The indeterminacy is removed throughout a region if one possesses a control profile as a boundary-condition. In the absence of such ground-truth, a point-boundary-condition will suffice only in conjunction with a heuristic assumption, such as that the strike-line runs perpendicularly to the line-of-sight. In the present study I have implemented a more reasonable assumption which I call 'the hypothesis of local cylindricity'.

Firstly, a general theory is derived, based solely on the implicit mathematical determinacy. This theory would be directly indicative of procedure if images were completely devoid of systematic error and noise. The theory produces topography by an area integration of radar brightness, starting from a control profile, without need of additional idealistic assumptions. But we have also theorized separately a method of forming this control profile, which method does require an additional assumption about the terrain. That assumption is that the curvature properties of the terrain are locally those of a cylinder of inferable orientation, within a second-order mathematical neighborhood of every point of the terrain. While local strike-and-dip completely determine the radar brightness itself, the terrain curvature determines the brightness-gradient in the radar image. Therefore, the control profile is formed as a line integration of brightness and its local gradient starting from a single point of the terrain where the local orientation of the strike-line is estimated by eye.

Secondly, and independently, the calibration curve for pixel brightness versus incidence-angle is produced. I assume that an applicable curve can be found from the literature or elsewhere so that our problem is condensed to that of properly scaling the brightness-axis of the calibration curve. A first estimate is found by equating the average image brightness to the point on the brightness axis corresponding to the complement of the effective radar depression-angle, an angle assumed given. A statistical analysis is then used to correct, on the one hand, for the fact that the average brightness is not the brightness that corresponds to the average incidence angle, as a result of the non-linearity of the calibration curve; and on the other hand, we correct for the fact that the average incidence angle is not the same for a rough surface as it is for a flat surface (and therefore not the complement of the depression angle).

Lastly, the practical modifications that were interactively evolved to produce an operational algorithm for treating real data are developed. They are by no means considered optimized at present. Such a possibility is thus far precluded by excessive computer-time. Most noteworthy in this respect is the abandonment of area integration away from a control profile. Instead, the topography is produced as a set of independent line integrations down each of the parallel range lines of the image, using the theory for control-profile formation. An adaptive technique, which now appears excessive, was also employed so that SEASAT images of sand dunes could be processed. In this, the radiometric calibration was iterated to force the endpoints of each profile to zero elevation. A secondary algorithm then employed line-averages of appropriate quantities to adjust the mean tilt and the mean height of each range profile. Following this step, a sequence of fairly ordinary filtering techniques was applied to the topography. An application is shown for a Motorola image of Crazy Jug Point in the Grand Canyon. Unfortunately, a radiometric calibration curve is unavailable. But a fictitious calibration curve has provided an encouraging qualitative test of these efforts.

Earth, Moon, and Planets **36** (1986) 217–247.

1. Introduction

The use of the photometric function of a surface for the purpose of translating image variegtion into slope and relief information dates back at least to the work of van Diggelen (1951), who applied it to lunar maria when near the terminator; a condition for which a uniquely simple limiting form of photometric function was inferred through the Helmholtz reciprocity principle (Minnaert, 1941). Based on the constancy of surface brightness near the bright limb of the Moon, this inference has since fallen into disrepute (Wildey, 1978).

The development of a method of producing a topographic map from a photometric image begins with Rindfleisch (1966), and independently with Watson (1968), who devised a theory which was implemented by Lambiotte and Taylor (1967). This process is as elaborate compared to the former one as photogrammetry is compared to basic trigonometric parallax. Accordingly, the term 'photoclinometry' was invented by Jack McCauley in 1965, from the greek roots 'photos' and 'klinos', in reference to this process; an event of which I have first-hand recollection.

For a given illumination and normal albedo of a terrain point under consideration, the photometric function enables the prediction of a measurable surface brightness as seen from any direction through the specification of three angles: g, the phase-angle, ϵ, the emergence angle, and i, the incidence angle. While the first angle can be independently known, the latter two depend on the orientation of the local surface normal (equivalent to knowledge of local strike-and-dip). Thus a knowledge of the local orientation of the terrain is essential to the prediction of surface brightness. In the inverse problem, where one has a measured surface brightness instead of known values of ϵ and i, one degree of freedom remains in the form of an implied functional relation between ϵ and i, rather than unique values thereof. The measured surface brightness imposes a constraint on the local normal vector, without uniquely determining it. It's range of possibilities generates a surface. This is the fundamental indeterminacy of photoclinometry. In the case of Watson's theory, uniquely applicable to the lunar surface, the indeterminacy could be ignored by confining the process to a one-dimensional rather than two-dimensional topographic mapping. The lunar photometric function, when particularly evaluated to correspond to the brightness of a single terrain-point, generates a locus of surface normals that is a plane perpendicular to the phase-plane. The measured surface brightness serves to specify the angular placement of the intersection of these two planes as a direction, as seen from the surface, algebraically between the direction to the illuminator and the direction to the observer. Watson showed that the intersection of the phase plane with the true surface, as a topographic profile, was uniquely determined by the variation in surface brightness along the corresponding line in the image. Unfortunately, no grounds exist for adjusting the relative range to two such profiles, which cannot intersect, taken from parallel data traverses in the same two-dimensional image.

In order to produce a two-dimensional topographic map purely by photoclinometry, the mathematical constraint imposed by an additional assumption is essential. There is no such thing as a completely reasonable assumption. But some assumptions are more absurd than others. One method of extending Watson's approach to two dimensions would be to adjust each parallel profile for a minimum of the integral of the square of height above an adopted lunar ellipsoid. While obviously not obeyed by the lunar surface, this assumption is also clearly superior to the assumption that the initial point on each profile is located precisely on the lunar ellipsoid.

The photometric functions characterizing most of the various martian terrain types are distinctly non-lunar in character. Any transformation of coordinates which might promote a single coordinate along which photoclinometric indeterminacy would disappear appears to involve the differential geometry of the topography itself as a Gaussian surface. Thus the first generalized two-dimensional photoclinometry was developed by Wildey (1974, 1975) in which the auxiliary assumption took the form of the Eulerian equations from the calculus-of-variations for the minimization of the total surface area. The analysis was mathematically interesting, the result plausible, and the algorithm eminently impractical.

An altogether different type of limitation on photoclinometry arises from the fact that planetary surfaces that are homogeneous in normal albedo are rare. Great strides toward the alleviation of this difficulty have recently been made by Eliason *et al.* (1981), who use multi-color image sets of the same terrain in an operations-research approach, to separate topography from albedo variation. Though representative of the greatest utility achieved to date to extract information in images due to topography, the auxiliary assumption used to render the photoclinometric portion of the study tractable was that the normal vector was confined to a plane containing the terrain point, the planetary center, and the Sun. The mathematical independence of parallel down-sun lines of integration of the topography produces a two-dimensional result with slopes in all directions, rather than merely toward the Sun. A Lambertian photometric function was also assumed. Thus the metric integrity of true photogrammetry was not approached. The separation of insolation and albedo variations is the important contribution of that work.

The primary goal of the present study has been the adaptation of photoclinometry to radar imagery, whether it be the type in which the reflected pulse generates all of a down-range raster in the final image (SLAR), or the type in which the reflected pulse, as complex electric amplitude, is but part of a contribution to a large synthesized optical aperture used to form the final image (SAR). The radar image as a candidate for photoclinometry offers both advantages and disadvantages, compared to ordinary optical images. Those considerations related to the simplicity of technique are, of course, less important than those considerations effecting the integrity of the result. The most obvious advantage is the simplicity of the photometric function. The radar becomes both the Sun and the camera, so that $g = 0$ and $i = \epsilon$. Any tabulated function of the single resulting angle i can be readily

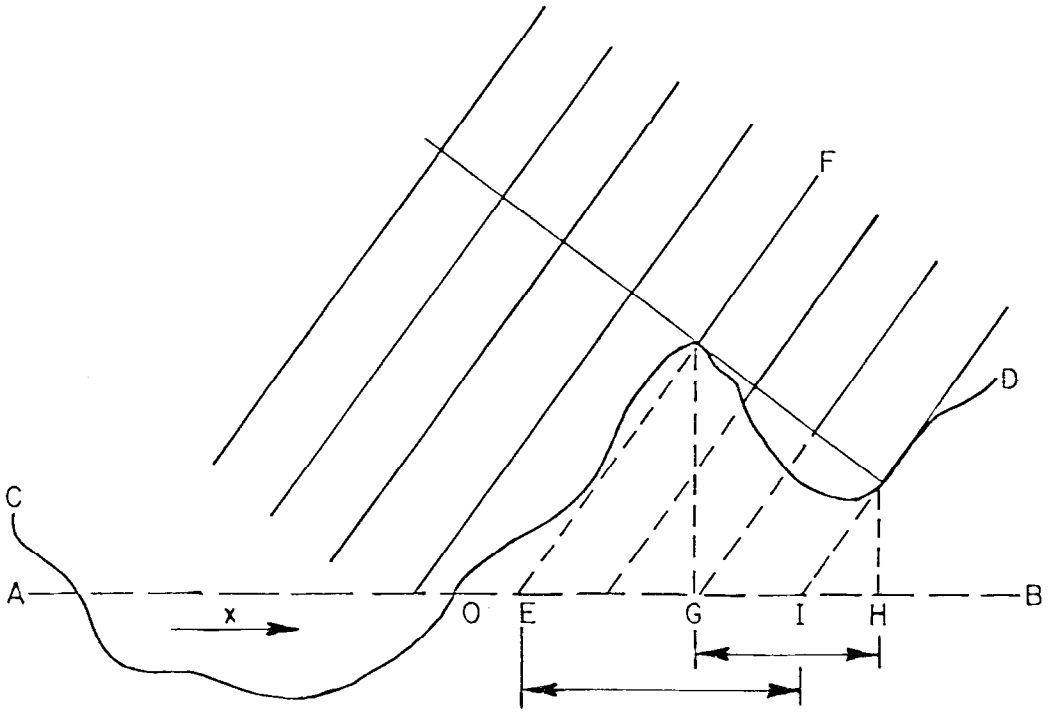

Fig. 1. Geometry of formation of the range-dependent coordinate, x, in a radar image.

accomodated. This, combined with the fact that radar imagery is essentially panoramic in nature, causes the surface brightness to have a dependence on the azimuthal component of slope that is zero to first order, as will be shown. Thus the consequences of ignoring this slope component in a down-range integration of topography are less severe. At the same time, however, the relative height adjustment of two such profiles adjacent to one another is made more uncertain by what is essentially poor photometric leverage. An additional advantage of radar stems from the subjective impressions that terrain homogeneous in radar albedo (normal back-scattering cross-section density) is more common than at visual wavelengths. For an objective evaluation of this, see Schaber *et al.* (1976) and Birrer *et al.* (1982).

Radar imagery presents one distinct complication over traditional optical imagery with respect to the physical nature of image coordinates. Photoclinometry is usually given serious consideration only when photogrammetry is impossible. That is, if the ratio of surface relief to camera range is so small that the relative parallax of features in all possible stereo-pairs is exceeded by image resolution, then photoclinometry offers the only possible source of topographic information. In the ensuing photoclinometric processing for the extraction of topography, no consideration need be given to a correction for mapping of a feature from image coordinates to coordinates on the mean-datum (mean-datum plane) because of the feature's height.

Such mapping simplicity can never exist in radar imagery because one image coordinate is essentially range itself. The problem is pictured in Figure 1. If the down-range coordinate is X, and the line AB represents an adopted mean-datum (apologies to photogrammetrists for the broadened use of this term), then the problem under consideration is represented by the lack of coincidence of the points E and G. Curve CD represents the topography. EF represents the crest of an electromagnetic wave just now reflecting from the summit of the promontory in the topography. The reflection will arrive back at the radar too soon and the peak will be 'mapped' to the point E in the radar image rather than the point G, which represents a true vertical projection onto the mean datum. (A worse case is represented by SEASAT radar in which the horizontal shift is over three-and-a-half times the height and one often sees a loss of one-to-one correspondence in mapping steep mountains.) The corner reflector at 0, whose height is zero, will appear at O. The horizontal separation between the reflector and the peak appears as OE rather than OG. The situation is not comparable to a vertically downward eyeball view of the terrain with the Sun at the same elevation angle as the radar. The solar shadow would lie to the right of G, but the radar shadow will lie to the right of E. They will have different lengths.

Probably the greatest disadvantage of radar in comparison to visual imagery lies in the area of the quality and uniformity of photometric (radiometric) calibration and the signal-to-noise ratio of a given digital element of surface brightness. At the very outset, relative photometric accuracy is limited by the repeatability of total transmitted pulse energy, an aspect of radar imagery incomparable to ordinary imagery. Image photometry (radiometry) has not been a traditional consideration in the design of radar imaging systems, nor in their corresponding signal-processing algorithms, especially when of an analog nature. In this connection SLAR possesses great advantage over SAR. On the one hand the power allocation to a final pixel is more generous in SLAR. But most especially, because SAR must preserve the electromagnetic wave's phase it suffers from 'speckle', a direct enhancement of the random error of pixel photometry, which can only be alleviated, from an engineering point of view, through the use of an unacceptably large number of 'looks'.

Throughout the sections which follow, it will be assumed that terrain homogeneous in 'radar albedo' is being processed.

2. Theory

A. RADIATIVE TRANSFER

Consider the following argument, which assumes perfect geometrical optics. Let a telescope form an image in the usual way of a terrain viewed obliquely. Let the telescope be sufficiently distant that the rays coming from the object are nearly an orthographic projection. Let the image plane in the telescope occur at the receiving surface of an array of equi-areal radiation sensors. Then the total radiative power

received by each sensor is the integral of the focal-plane flux over the intercepting area of each sensor. Next consider the mapping of all the rays from the boundary of an arbitrarily chosen sensor, through the telescope, to their intersection with the terrain. In the immediate vicinity of the ground, the locus of these rays is a mathematical closed-cylinder; and its intersection with a plane perpendicular to the rays forms a closed curve bounding an area of integration for contribution to the total radiative power received by the sensor. The quantity to be integrated will be the specific intensity, or surface-brightness, (watts/meter^2/steradian) emerging from the terrain into the direction of the telescope, multiplied by the solid-angle subtended at a point in the area of integration by the area of the telescope aperture. Given the constancy of the aforementioned solid angle, energy conservation dictates that the image-plane flux is directly proportional to, and a mapping of, the specific intensity distribution over a plane perpendicular to the line-of-sight near the ground. Given also that the sensors have equal receiving areas and are dynamically identical and linear, the DN values in the resulting digital image will be directly proportional to the specific-intensity in the proper direction at the corresponding point of the viewed surface.

If the foregoing picture is replaced by one in which a microwave CW transmitter and receiver pair, of very narrow and symmetric main lobe in the antenna-pattern, operates by serially positioning itself at points in a two-dimensional raster of equally spaced *angular* directions, whose spacing is at least as large as the entenna pattern, then a digital image results about which the same conclusion can be made. Here it depends on the constancy of transmitter power, the accurate ability of the receiver to measure power, and, of course, the constancy of effective antenna area.

The situation is rather more complicated when we examine radar images. The apparently simplest to consider initially is the SLAR, or brute-force radar, which at least presents some similarity to the CW picture with regards to one of the dimensions (azimuth). Let us consider first, in fact, a truly idealized version of the 'brute-force' technique, in which the azimuthal resolution is not only directly the width of the antenna pattern, but the range resolution is directly the length of the transmitted radar pulse, and the matched dwell-time of the receiver detecting the returned waveform. In this view, the power, or more precisely the energy, that is allocated to the DN number of a given image pixel all comes from a range-interval, approximately also the range resolution, that is a constant of the image frame. The width in azimuth of this resolution-cell is also a constant of the frame. The difficulty in identifying the DN value of a pixel in a radar frame as proportional to the specific intensity of reflected radar radiation back-scattered from the corresponding point on the ground is thus seen to be a result of the fact that an image resolution cell does not map into a constant area in the plane near the ground that is perpendicular to the line-of-sight. Thus the emergent specific intensity, though always multiplied by a constant solid angle, is multiplied by a variable area, in forming the energy that is transduced into the DN value of a pixel. In fact the geometry of the situation reveals that the

boundaries of the integrating area for the specific intensity that correspond to the range-resolution-interval, Δr, are *separated* by the distance $\Delta r \cot i$, where i is the local incidence angle of the terrain. These boundary lines are perpendicular to the plane containing the local normal to the terrain and the line of sight from the radar to the terrain point. If the constant azimuthal interval, Δy, corresponding to azimuthal resolution is bounded by two loci of constant azimuth, they will cut the two range-related lines so as to form a small parallelogram as the area for specific-intensity integration. The azimuth-related lines will have separation, Δy. But this makes the area of the parallelogram $\Delta r \Delta y \cot i \sec \varphi$, where φ is the position angle of the local normal with respect to the local vertical as seen from the radar. While $\Delta r \Delta y$ is a constant, $\cot i \sec \varphi$ is not. In certain limits, this effective integration-area for the specific intensity achieves infinite dimensions. Of course the finite limits of antenna pattern will cut off any such effects, and the differential treatment of the local terrain will fail even sooner. Insofar as $\sec \varphi$ is never far from 1, it can be neglected. In that case, a backscatter-intensity versus incidence angle curve obtained from CW active microwave measurements proposed to provide a photometric function for radar photoclinometry need only be multiplied by $\cot i$ in order to provide an effective curve that may be applied *as though* the DN values in the radar image were proportional to 'specific intensity'. Of course linear transduction must still hold. The foregoing picture may also be oversimplified when applied to aperture-synthesis in terms of an effective Δr and Δy. As parallel efforts by others in the development of calibrated imaging radars achieve fruition, we will be justified in removing this largely heuristic limitation. Such is planned for future continuing investigations.

B. DIFFERENTIAL GEOMETRY

Photoclinometry is quite generally described by an inhomogeneous non-linear first-order partial differential equation in the topography, considered in the form of height-above-mean-datum, z, as a function of cartesian coordinates x and y on the mean datum. Consider any photometric function, $\Phi(g, i, \epsilon)$. Let the topography be given by $z = z(x, y)$. In three dimensions, the topography can be viewed in terms of an equipotential surface

$$V(x, y, z) = z - z(x, y) = 0, \tag{1}$$

where z appears in the dual context of independent variable and name of a function. The gradient of this potential function will point perpendicularly to the equipotential surface, i.e., the topography: i.e.,

$$\nabla V = -\frac{\partial z}{\partial x}\hat{i} - \frac{\partial z}{\partial y}\hat{j} + \hat{k}, \tag{2}$$

The unit normal vector which will always have a positive z component is then given by

$$\hat{n} = \frac{-\frac{\partial z}{\partial x}\hat{i} - \frac{\partial z}{\partial y}\hat{j} + \hat{k}}{\sqrt{1 + \left(\frac{\partial z}{\partial x}\right)^2 + \left(\frac{\partial z}{\partial y}\right)^2}}. \tag{3}$$

Let unit vectors $\hat{e}$ and $\hat{s}$ point toward the observer and the illuminator, respectively. They may or may not be nearly constant vectors in an image, but they are in any event known functions of no more than x and y. The same may be said of the phase angle, g. Now we will have

$$\cos \epsilon = \hat{e} \cdot \hat{n}, \tag{4}$$

$$\cos i = \hat{s} \cdot \hat{n}. \tag{5}$$

If we now let the given specific intensity of the image, transformed if necessary, be $b(x, y)$; doing photoclinometry consists in solving the equation

$$\Phi(g, i, \epsilon) = Cb(x, y) \tag{6}$$

for the function $z(x, y)$, where C is a calibration constant dependent on the illuminating flux and the normal albedo. Because g, i, and ϵ depend on x, y, $\partial z/\partial x$, $\partial z/\partial y$, $(\partial z/\partial x)^2$, and $(\partial z/\partial y)^2$ through Equations (3), (4), and (5), Equation (6) is a non-linear first-order partial differential equation with a driving function, $Cb(x, y)$. In the corresponding numerical analysis, an equation involving both first derivatives is a triangular 3-point condition on a corresponding integration mesh of discrete values of x and y. If a single profile in z is given for all x at a constant value of y, profiles in x for the adjacent values of y may be generated. Thus the fundamental indeterminacy of photoclinometry reduces to the requirement of a one-dimensional boundary condition. Because the equations are non-linear and driven, and only real values of z are meaningful, the boundary condition cannot be specified arbitrarily and independently. We may also use the lunar example to note that the boundary profile may not necessarily be sufficient if arbitrarily directed, e.g., in the phase-plane.

Let us now direct ourselves specifically toward radarclinometry. Because $\Phi = \Phi(\epsilon)$, for a given C, the image may be readily conceived directly as cosine of incidence angle, rather than specific intensity. Let $\mu = \cos i$. Then Equation (6) becomes

$$\hat{e} \cdot \hat{n} = \mu(x, y) \tag{7}$$

or

$$\frac{e_z - e_x\frac{\partial z}{\partial x} - e_y\frac{\partial z}{\partial y}}{\sqrt{1 + \left(\frac{\partial z}{\partial x}\right)^2 + \left(\frac{\partial z}{\partial y}\right)^2}} = \mu(x, y),$$

which is more readily useable in standard quadratic form

$$\{[\mu(x, y)]^2 - e_y{}^2\}\left(\frac{\partial z}{\partial y}\right)^2 - 2\,e_y\left(e_x\frac{\partial z}{\partial x} - e_z\right)\frac{\partial z}{\partial y} + \\ + \left\{[\mu(x, y)]^2\left[1 + \left(\frac{\partial z}{\partial x}\right)^2\right] - \left(e_x\frac{\partial z}{\partial x} - e_z\right)^2\right\} = 0. \tag{8}$$

A further simplification is possible, with a proper choice of coordinates, due to the inherently panoramic nature of radar imagery. Let us choose the x axis positive directly downrange from the radar position. Let the positive y axis point in the direction of motion of the radar platform. It will then always turn out for all x and y that $e_y = 0$.

Equation (8) can be quickly solved to yield

$$\frac{\partial z}{\partial y} = \pm\sqrt{\left(\frac{e_x\frac{\partial z}{\partial x} - e_z}{\mu}\right)^2 - \left[1 + \left(\frac{\partial z}{\partial x}\right)^2\right]}. \tag{9}$$

Let σ and ν be integers identifying the numerical lattice of integration. If one is at point (x_σ, y_ν) on a boundary profile or the profile of an immediately preceding integration, $\partial z/\partial x$ is formed from $(z_{\sigma+1,\nu} - z_{\sigma,\nu})/(x_{\sigma+1} - x_\sigma)$, while μ, e_x, e_z are known. Formula (9) then yields $\partial z/\partial y$; and the value of z at the mesh point $(x_\sigma, y_{\nu+1})$ is then increased over the value at (x_σ, y_ν) by Δy times this amount.

As mentioned earlier, x and y are the true coordinates of features on the mean datum. They are the ultimately preferred coordinates. In terms of image coordinates, x' and y', we must use the transformation derivable from Figure 1:

$$y' = y, \qquad x' = x - z(x, y)\tan\alpha, \tag{10}$$

where α is the depression angle of the radar, and $\tan\alpha = -e_z/e_x$. The elements of the Jacobeans for the direct and inverse transformations are:

$$\frac{\partial x'}{\partial x} = 1 + e_z/e_x\frac{\partial z}{\partial x},$$

$$\frac{\partial x'}{\partial y} = e_z/e_x\frac{\partial z}{\partial y},$$

$$\frac{\partial y'}{\partial x} = 0,$$

$$\frac{\partial y'}{\partial y} = 1, \tag{11}$$

$$\frac{\partial x}{\partial x'} = \frac{1}{1 + e_z/e_x\frac{\partial z}{\partial x}},$$

$$\frac{\partial x}{\partial y'} = -\frac{e_z/e_x \dfrac{\partial z}{\partial y}}{1 + e_z/e_x \dfrac{\partial z}{\partial x}}$$

$$\frac{\partial y}{\partial x'} = 0,$$

$$\frac{\partial y}{\partial y'} = 1.$$

One integrates in the domain of the image, accumulating the necessary transformation to ensure that each new value of z is put in proper correspondence with x and y. The sign ambiguity in Equation (9) can be resolved by making the rather reasonable assumption that the local isophote describes a surface line-element along which the normal vector is locally unchanging. If the isophotic direction is compared with the sign of $\partial z/\partial x$ as found from the current profile, a reasonable sign for $\partial z/\partial y$ can be found. For example, if the isophote trends from $(-, -)$ to $(+, +)$ in the x', y' plane, and $\partial z/\partial x$ is locally positive, then $\partial z/\partial y$ should be negative.

The foregoing analysis represents an operationally complete scheme, in principle, and emphasizes the requirement for one-dimensional ground-truth. It seems reasonable to suppose that if one can supply such a boundary profile, one has sufficient technology at one's disposal as to make reliance on photoclinometry unnecessary in any event. We therefore need to consider auxiliary mathematical assumptions that will enable the generation of such a boundary profile from initial point conditions photoclinometrically. Assuming that all slopes along a line of constant y are either directly toward or away from the radar seems unacceptable. One does not obtain the correct down-radar slope to the exclusion of the cross-radar slope when one does this. $\partial z/\partial x$ and $\partial z/\partial y$ are not mathematically separable in the equations of photoclinometry. One simply obtains the wrong value of $\partial z/\partial x$. Mental reflection regarding radarclinometry performed on a hemispherical convexity, employing such a simplistic assumption, reveals that the profile which bisects the structure will be correct. For all parallel profiles the slopes down-radar will be underestimated (effectively rotating $\hat{n}$ about $\hat{e}$ into the vertical plane) so that the derived structure will have a ridgeline oriented down-range with depressed sides. A bilaterally symmetric ridge, or convex mathematical cylinder, trending obliquely, would be scaled down non-linearly in the vertical dimension and the flat terrain on the opposite sides would separate in elevation.

Let's begin this search for a reasonable auxiliary assumption by examining the significance of information expansion in the form of not only the value of μ at each x' and y' in the image but of the two-dimensional gradient of μ as well. We will need the components expressed in terms of the coordinates on the mean-datum. By the chain-rule,

$$\frac{\partial \mu}{\partial x} = \frac{\partial \mu}{\partial x'}\frac{\partial x'}{\partial x} + \frac{\partial \mu}{\partial y'}\frac{\partial y'}{\partial x},$$

$$\frac{\partial \mu}{\partial y} = \frac{\partial \mu}{\partial x'}\frac{\partial x'}{\partial y} + \frac{\partial \mu}{\partial y'}\frac{\partial y'}{\partial y}. \tag{12}$$

In Equations (12), the derivatives with respect to x' and y' are directly the pixel differences in the image, and other derivatives are from Equations (11). Equations (12) represent the transformed measurements which apply. We have, on the other hand, the theoretical equivalents of the left-hand-sides of Equations (12) obtained by differentiating Equation (7) with e_y set to zero: i.e.,

$$\frac{\partial \mu}{\partial x} = \left[1 + \left(\frac{\partial z}{\partial x}\right)^2 + \left(\frac{\partial z}{\partial y}\right)^2\right]^{-3/2} \left\{\left(e_x \frac{\partial z}{\partial x} - e_z\right)\frac{\partial z}{\partial y}\frac{\partial^2 z}{\partial x \partial y} - \right.$$

$$\left. - e_x\left[\left(\frac{\partial z}{\partial y}\right)^2 + 1\right]\frac{\partial^2 z}{\partial x^2} - e_z \frac{\partial z}{\partial x}\frac{\partial^2 z}{\partial x^2}\right\},$$

$$\frac{\partial \mu}{\partial y} = \left[1 + \left(\frac{\partial z}{\partial x}\right)^2 + \left(\frac{\partial z}{\partial y}\right)^2\right]^{-3/2} \left\{\left(e_x \frac{\partial z}{\partial x} - e_z\right)\frac{\partial z}{\partial x}\frac{\partial^2 z}{\partial y^2} - \right.$$

$$\left. - e_x\left[\left(\frac{\partial z}{\partial y}\right)^2 + 1\right]\frac{\partial^2 z}{\partial x \partial y} - e_z \frac{\partial z}{\partial x}\frac{\partial^2 z}{\partial x \partial y}\right\}. \tag{13}$$

We do not expect that merely looking at the gradient introduces determinacy, and that is surely the case, for by adding the *two* gradient equations we have introduced *three* unknown second derivatives not present in our original Equation (7). Thus, instead of promoting determinacy we have now, on the contrary, a theory with two remaining degrees of freedom instead of one. The '*hypothesis-of-local-cylindricity*' will now be invoked. The second derivatives now involved in the argument describe fully the local curvature properties of the topography. We will assume the curvature is *locally* cylindrical in nature, of arbitrary orientation. That is, there exists a direction in space in which the curvature is maximum and another direction perpendicular to the first in which it is zero. This defines a local tangent plane to the topography. The local curvature in all other directions in the plane is a projection of the maximum. Thus is defined a local tangent cylinder of equivalent local curvature as well. I emphasize that this is a *local* and not a *global* assumption about the topography. To be reasonable, it is only necessary that local curvature possess a fairly dominant direction. Aside from such features as granite domes and the summits of mountain peaks, local-cylindricity (LC) seems to me to be fairly consistent with topography on the Earth, probably due to the dominance of down-slope movement in the erosion-transport process. If the hypothesis tends to fail the more as curvature of any kind becomes slight, there is compensation in the fact that it means local slope is changing negligibly from an already established value.

What are the consequences of LC for the equations at hand? Consider an alternative set of x and y axes, say x'' and y'', that are rotated about the z axis with respect to x and y. Assuming that LC prevails, let the axis of the local tangent-and-equivalently-curved cylinder be parallel to the $y''z$ plane. It may have an arbitrary axial elevation angle. The following facts then follow from LC.

$$\begin{aligned} &\frac{\partial z}{\partial y''} \neq 0, && && \\ &\frac{\partial z}{\partial x''} \neq 0; && \text{but} && \frac{\partial^2 z}{\partial y''^2} = 0, \\ &\frac{\partial^2 z}{\partial x''^2} \neq 0. && && \frac{\partial^2 z}{\partial x'' \partial y''} = 0. \end{aligned} \tag{14}$$

Let the angle of rotation into the (x, y, z) system from the (x'', y'', z) system be θ. The transformation matrix for 2-dimensional vectors defined in the (x, y) plane is thus given by

$$\gamma_{\sigma\nu} = \begin{pmatrix} \cos\theta & \sin\theta \\ -\sin\theta & \cos\theta \end{pmatrix}. \tag{15}$$

Now the topography certainly has a physical meaning independent of the coordinate system used to represent it. Its functional representation is a true scalar in the group-theoretical sense. Its second derivatives therefore have a second-rank tensor character and the appropriate transformation laws may be used to re-represent the set of values shown in Equations (14) in terms of x and y as

$$\frac{\partial^2 z}{\partial x_\xi \partial x_\eta} = \sum_{\substack{\sigma=1 \\ \nu=1}}^{2,2} \gamma_{\xi\sigma}\, \gamma_{\eta\nu} \frac{\partial^2 z}{\partial x_\sigma \partial x_\nu}. \tag{16}$$

If we let σ and ν each refer to the (x'', y'') system and ξ and η each refer to the (x, y) system, applying Equation (16) using the values shown in Equations (15) and (14) we have

$$\begin{aligned} \frac{\partial^2 z}{\partial x^2} &= \cos^2\theta \frac{\partial^2 z}{\partial x''^2}, \\ \frac{\partial^2 z}{\partial x \partial y} &= -\sin\theta\cos\theta \frac{\partial^2 z}{\partial x''^2}, \\ \frac{\partial^2 z}{\partial y^2} &= \sin^2\theta \frac{\partial^2 z}{\partial x''^2}; \end{aligned} \tag{17}$$

the essential importance of which is that it leads to the conclusion that there exists a parameter λ, which we may identify as $\tan\theta$, such that

$$\frac{\partial^2 z}{\partial x \partial y} = -\lambda \frac{\partial^2 z}{\partial x^2} \quad \text{and} \quad \frac{\partial^2 z}{\partial y^2} = \lambda^2 \frac{\partial^2 z}{\partial x^2}. \tag{18}$$

In Equations (18) one quickly sees that the three unknown second derivatives have been traded for two unknown values of λ and $\partial^2 z/\partial x^2$. Equations (18) can be used to substitute into Equations (13). Thus we have reduced two remaining degrees of freedom back to one.

The parameter λ deserves deeper inquiry. It is the tangent of the angle, as we have seen, between the y axis and the projection of the local cylindrical axis onto the mean datum. The line in the surface that is in the cylindrical-axial direction must be a locus of constant $\hat{n}$. As such, its image must be an isophote. In terms of the image mapping in x and y, we therefore conclude:

$$\lambda = -\left(\frac{\partial \mu}{\partial y}\right) \Big/ \left(\frac{\partial \mu}{\partial x}\right). \tag{19}$$

This follows from the requirement that $d\mu = 0$ along the line-element for which $dy/dx = 1/\lambda$. In terms of the directly measured gradient in the image, using the chain rule and Equations (11), we have

$$\lambda = -\left[\left(\frac{\partial \mu}{\partial y'}\right) \Big/ \left(\frac{\partial \mu}{\partial x'}\right) + e_z / e_x \frac{\partial z}{\partial y}\right] \Big/ \left(1 + e_z / e_x \frac{\partial z}{\partial x}\right) \tag{20}$$

With the appearance of Equation (20), the illusion is created that we have finally arrived at complete determinacy of all first and second derivatives. One extra equation has been found to account for the remaining degree of freedom. Such is not the case. If we combine Equations (11), (12), and (13), and substitute for the mixed derivative and the second derivative with respect to y from Equations (18), thereafter eliminating the parameter λ thus introduced by substitution from Equation (20), and finally eliminating the radical by substitution for it from Equation (7), we extract the following two equations for the two components of the image gradient:

$$\begin{aligned} &\mu^{-3}\left(\frac{\partial \mu}{\partial x'}\right)^2 \left(e_z - e_x \frac{\partial z}{\partial x}\right)^3 \left(1 + e_z e_z^{-1} \frac{\partial z}{\partial x}\right)^2 + \\ &+ \frac{\partial \mu}{\partial y'}\left(e_z - e_x \frac{\partial z}{\partial x}\right) \frac{\partial z}{\partial y} \frac{\partial^2 z}{\partial x^2} + e_x^{-1} \frac{\partial \mu}{\partial x'}\left[e_z^2 \left(\frac{\partial z}{\partial x}\right)^2 + \right. \\ &\left. + \left(\frac{\partial z}{\partial y}\right)^2\right] \frac{\partial^2 z}{\partial x^2} + \frac{\partial \mu}{\partial x'}\left(e_x + 2e_z \frac{\partial z}{\partial x}\right) \frac{\partial^2 z}{\partial x^2} = 0; \end{aligned} \tag{21}$$

and a second equation which turns out to be none other than Equation (21) multiplied on the left-hand-side by the factor

$$\frac{\partial \mu}{\partial y'} + e_z e_x^{-1} \frac{\partial \mu}{\partial x'} \frac{\partial z}{\partial y}.$$

Thus the LC hypothesis does not result in a set of equations which are algebraically determinant. It *does*, however, result in a set of equations which are *one-dimensionally* integrable starting from a *point* boundary condition. They therefore complement the earlier set of non-LC equations which are two-dimensionally in-

tegrable starting from a line boundary condition. That Equations (12) and (13) did not produce two independent equations in the end is not too surprising. One certainly expects to identify image-brightness gradient with surface curvature, but a one-to-one correspondence is achieved only with a *projection* of the latter into the two-dimensional space of the image, even after the LC hypothesis is used to equalize the number of independent components of the two entities. A knowledge of λ constrains the rotational orientation of the projected line in the image, but the projection scaling remains unknown. The mapping peculiarities of radar do not ameliorate this limitation on determinacy.

In principle, then, the integration of an entire topography can now proceed as follows. We may define the basic quantity which is stepped in the integration producing the boundary profile as the ratio of the slope components

$$\eta = \left(\frac{\partial z}{\partial y}\right) \Big/ \left(\frac{\partial z}{\partial x}\right),$$

which must be specified initially be eyeball estimate, though the influence of the starting value on the subsequent course of profile development is somewhat stochastic. Equation (7) may be rewritten in terms of $\partial z/\partial x$ and η as

$$[\mu^2 (1-\eta^2) - e_x^2] \left(\frac{\partial z}{\partial x}\right)^2 + 2e_z e_x \frac{\partial z}{\partial x} + (\mu^2 - e_z^2) = 0. \tag{22}$$

For a given value of η that is either the starting value or the current value from the last integration step, one solves Equation (22), using the immediate image datum, μ, for $\partial z/\partial x$. Discrimination between the two roots of the quadratic is on the basis that no slope steeper than the incident wave plane of the radar has been admitted into the processing. With η known, $\partial z/\partial y$ immediately follows. These two slope components together with the immediate pixel differences, $\partial\mu/\partial x'$ and $\partial\mu/\partial y'$, can be inserted into Equation (21) which is then easily solved for $\partial^2 z/\partial x^2$. One then uses Equation (20) to find λ, and one of Equations (18) to find $\partial^2 z/\partial x \partial y$. We now step to the next integration point as

$$\begin{aligned}
\frac{\partial z}{\partial x} &\to \frac{\partial z}{\partial x} + \frac{\partial^2 z}{\partial x^2}\Delta x, \\
\frac{\partial z}{\partial y} &\to \frac{\partial z}{\partial y} + \frac{\partial^2 z}{\partial x \partial y}\Delta x, \\
\eta &\to \frac{\dfrac{\partial z}{\partial y} + \dfrac{\partial^2 z}{\partial x \partial y}\Delta x}{\dfrac{\partial z}{\partial x} + \dfrac{\partial^2 z}{\partial x^2}\Delta x}, \\
z &\to z + \frac{\partial z}{\partial x}\Delta x + \frac{1}{2}\frac{\partial^2 z}{\partial x^2}(\Delta x)^2.
\end{aligned} \tag{23}$$

The process can now be repeated. An important acknowledgement is necessary in order that a local strike-line may evolve successfully through the plane containing the local vertical and radar line-of-sight. It will be noted that η is not updated through a differential formula, but from new values of the slope components that are thus linearized individually and updated. It would not otherwise be possible for η to pass through the perfectly meaningful discontinuity ($+\infty \leftrightarrow -\infty$). While $\partial z/\partial x$ and $\partial z/\partial y$ are continuous variables, η is simply a discrete set.

When the boundary profile is complete, one proceeds according to the non-LC approach described in the first part of this section. Presumably the integration mesh is constant in x' rather than x, so that one operates pixel-to-pixel in the image. The value of Δx in the foregoing is therefore given by

$$\Delta x = \frac{\partial x}{\partial x'} \Delta x' + \frac{1}{2} \frac{\partial^2 x}{\partial x'^2} (\Delta x')^2, \tag{24}$$

where the second order term is available because topographic second derivatives have been determined. Noting that $\partial x/\partial x'$ is a function of $\partial z/\partial x$ in Equations (11), one writes by virtue of the chain-rule

$$\frac{\partial^2 x}{\partial x'^2} = - \frac{e_z / e_x}{1 + e_z/e_x \dfrac{\partial z}{\partial x}} \left(\frac{\partial^2 z}{\partial x^2} \frac{\partial x}{\partial x'} + \frac{\partial^2 z}{\partial y \partial x} \frac{\partial y}{\partial x'} \right), \tag{25}$$

whose parameters are known every step of the way.

3. Calibration

A radar back-scattering curve with a *relative* scattering cross-section scale must be independently available, together with a knowledge of the radar's depression angle, α, so that e_x and e_z may be determined. If the radar frame is wide-field, that information is necessary to compute the variation in α and $\hat{e}$ over the frame. Beyond this, only the digitized radar frame itself is needed. That frame *is* desirably the most photometric rendition of the *relative* strength of true radar surface-brightness and not merely a monotonic substitute.

Given the above, the simplest approach to the evaluation of C in Equation (6), where $\Phi(g, i, \epsilon)$ is now simply $\varphi(i)$, would be to evaluate $\langle b \rangle$, the average brightness for the entire frame, and then take C as $\varphi(\pi/2 - \alpha)/\langle b \rangle$. This assumes that the average incidence angle of the *terrain* is the same as that of the mean-datum, which is not true for a rough surface that is statistically isotropic in x and y. It is especially untrue considering the fact that isotropy on the mean datum transforms to anisotropy in the picture domain. In addition it assumes that $\varphi(i)$ is approximately linear over the range about $i = \pi/2 - \alpha$ that was significant in producing the variations in b.

Accordingly, this first-order calibration is given a small iteration arrived at in the following manner. Let A be any locally defineable property of the terrain. Thus A may be considered a function of x and y (or x' and y' for that matter). We shall

subsequently want A to represent μ and μ^2. Let A also be functionally determined by the local components of slope, $\partial z/\partial x$ and $\partial z/\partial y$, which we shall temporarily refer to as z_x and z_y, in order to avoid some unwidely expressions. We will assume that the probability distribution for slopes is isotropic and gaussian as related to sampling that is uniform on the mean-datum.

$$P(z_x, z_y) = \frac{1}{2\pi\sigma} e^{-} \exp[-(z_x^2 + z_y^2)/2\sigma. \tag{26}$$

Accordingly, we will have alternative prescriptions for the average value of A.

$$\langle A \rangle = \int_{-\infty}^{+\infty} \int_{-\infty}^{+\infty} P(z_x, z_y)\, A(z_x, z_y)\, \mathrm{d}z_x\, \mathrm{d}z_y, \tag{27}$$

$$\langle A \rangle = \int_{y_1}^{y_2} \int_{x_1}^{x_2} A(x, y)\, \mathrm{d}x\, \mathrm{d}y \,/\, [(y_2 - y_1)\,(x_2 - x_1)], \tag{28}$$

If we take an average over a radar picture-frame we do not have the kind of average indicated in Equations (27) and (28), because we are not sampling uniformly on the mean-datum. We know that slopes toward the radar are rendered in diminished duration compared to slopes away from the radar. If we let $P'(z_x, z_y)$ be a corresponding probability distribution for uniform sampling over the radar image-frame, then the average value we will measure, for example, of μ, by converting brightnesses, pixel-by-pixel, to μ and summing line-by-line over the frame, would be represented by substituting P' for P in Equation (27) and x' for x and y' for y in Equation (28). Our immediate problem is to find P'. In order to do this we must rethink Equation (27) as a condensed integral over the actual slopes of the surface, with P representing the normalized multiplicity of distinct pairs of z_x and z_y. If Equation (28) is mapped from the space of x and y to the space of z_x and z_y, the result can be called the equivalent of Equation (27) and interidentification of terms can be achieved. In order to do this properly the integral of Equation (28) should be divided up into however many integrals over separate domains are required in order that a one-to-one mapping between each individual domain in x and y and the single domain in z_x and z_y is achieved. Let n label such a domain and let there be a total of N of them. Inasmuch as the domains are contiguous, then, the leading reciprocal of integration-range in Equation (28) is unaffected and the equation becomes

$$\langle A \rangle = (y_2 - y_1)^{-1}\,(x_2 - x_1)^{-1} \sum_{n=1}^{N} \int_{y_{1n}}^{y_{2n}} \int_{x_{1n}}^{x_{2n}} A(x, y)\, \mathrm{d}x\, \mathrm{d}y, \tag{29}$$

the mapped form of which is given by

$$\langle A \rangle = (y_2 - y_1)^{-1}\,(x_2 - x_1)^{-1} \sum_{n=1}^{N} \int_{z_{y1n}}^{z_{y2n}} \int_{z_{x1n}}^{z_{x2n}} A(z_x, z_y) \left[\frac{\partial(x, y)}{\partial(z_x, z_y)}\right]_n \mathrm{d}z_x\, \mathrm{d}z_y.$$

The Jacobian of the foregoing equation is the reciprocal of the one whose elements are the second derivatives of the surface function, z; and its behavior in any one domain is independent of its behavior in all the others, so that it can properly be given a subscript, n. Equation (29) inter-identifies with Equation (27) and would constitute the empirical basis for the probability distribution, P, whose form we have assumed. The original integration relating to P is defined on the mean datum. We may find P' by combining this result with the result of the same procedure applied to mapping the integration over the radar image-frame into the space of z_x and z_y. Remember that z_x and z_y still represent $\partial z/\partial x$ and $\partial z/\partial y$; not $\partial z/\partial x'$ nor $\partial z/\partial y'$. The repeat performance yields

$$\langle A \rangle' = (y_2' - y_1')^{-1} (x_2' - x_1')^{-1} \sum_{n=1}^{N'} \int_{z_{y'1n}}^{z_{y'2n}} \int_{z_{x'1n}}^{z_{x'2n}} \times$$

$$\times A(z_x, z_y) \left[\frac{\partial(x', y')}{\partial(z_x, z_y)} \right]_n dz_x \, dz_y, \tag{30}$$

which inter-identifies with Equation (27) written with P' substituted for P. If the Jacobians for the transformations between (x, y) and (x', y'), both direct and inverse, vanish nowhere in the regions of interest (there are no terrain slopes steeper than the radar wavefront) then the topological relations between the slope domain and the mean datum are the same as between the slope domain and the image-frame. Therefore $N' = N$ and the individual domains in Equation (29) can be inter-identified with those of Equation (30) on a one-to-one basis.

Now the probability, P, under discussion, can be interpreted as a sum of individual probabilities, P_n, each one of which is a joint probability of (1) being in the domain n, and (2) the slope probability distribution applicable to the particular domain. This enables the detailed inter-identification between Equations (27) and (29) to be given by

$$P_n = (y_2 - y_1)^{-1} (x_2 - x_1)^{-1} \left[\frac{\partial(x, y)}{\partial(z_x, z_y)} \right]_n ;$$

and, similarly,

$$P_n' = (y_2' - y_1')^{-1} (x_2' - x_1')^{-1} \left[\frac{\partial(x', y')}{\partial(z_x, z_y)} \right]_n .$$

We assume that the frame is sufficiently large that there is negligible difference in *overall* integration ranges, i.e., $y_2' - y_1' = y_2 - y_1$ and $x_2' - x_1' = x_2 - x_1$. And therefore,

$$P_n' = P_n \left[\frac{\partial(x', y')}{\partial(z_x, z_y)} \right]_n \Big/ \left[\frac{\partial(x, y)}{\partial(z_x, z_y)} \right]_n ;$$

But by Jacobi's theorem, the ratio of the two Jacobians is

$$\left[\frac{\partial(x', y')}{\partial(x, y)}\right]_n.$$

A quick glance at Equations (11) reveals that this Jacobian is uniquely defined by the values of z_x and z_y at the point of the contribution to the integral over z_x and z_y, so that the subscript n is no longer necessary or significant. Factorization is therefore possible, resulting in

$$P' = \sum_{n=1}^{N} P'_n = \frac{\partial(x', y')}{\partial(x, y)} \sum_{n=1}^{N} P_n$$

or

$$P'(z_x, z_y) = P(z_x, z_y) \frac{\partial(x', y')}{\partial(x, y)}; \tag{33}$$

$$P'(z_x, z_y) = \left(\frac{1 + e_z z_x/e_x}{2\pi\sigma}\right) \exp\left[-(z_x^2 + z_y^2)/2\sigma\right], \tag{34}$$

With this expression for P' substituted for P in Equation (27), we may compute $\langle\mu\rangle$ and $\langle\mu^2\rangle$ in terms of σ, using Equation (7).

Now it is also possible to compute directly from the data, using the provisional calibration, the frame average values of $\langle\mu\rangle$ and $\langle\mu^2\rangle$. The provisional calibration is based on setting the average brightness in correspondence with e_z. Even if $\langle\mu\rangle = e_z$ in reality, the non-linearity of the calibration curve will cause the $\langle\mu\rangle$ read out of the data in this way to be different from e_z. Let us denote by φ the photometric function that has μ, instead of i, as its arguments. Then according to the provisional calibration,

$$\langle b\rangle = C\varphi(e_z).$$

We have a $\langle\mu\rangle$ computed from the data through this provisional calibration which we'll call $\langle\mu\rangle_0$, from which we obtain a value b_0.

$$b_0 = C\varphi(\langle\mu\rangle_0).$$

Now if we believe $\langle\mu\rangle$ actually should be e_z, we may make a correction to C in that direction by adopting as the new value of C, $b_0/\varphi(e_z)$.

With the correction for the non-linearity of the photometric function thus established, the correction for the fact that $\langle\mu\rangle \neq e_z$ can now be made. The calculations using Equations (34), (27), and (7) need be carried out only to 2nd order in z_x and z_y, for the non-exponential factors in the integrands. The results are

$$\langle\mu^2\rangle = e_z^2 - (4e_z^2 - e_x^2)\sigma \quad \text{and} \quad \langle\mu\rangle = e_z(1 - 2\sigma),$$

from which, to 2nd order,

$$\sigma = \langle(\Delta\mu)^2\rangle/e_x^2. \tag{35}$$

We therefore calculate σ in Equation (34) from the frame averages, $\langle(\Delta\mu)^2\rangle = \langle\mu^2\rangle - \langle\mu\rangle^2$, and then use it to revise $\langle\mu\rangle$ from the immediately preceding equation. We finally revise our calibration constant by multiplying it by the ratio $\varphi(e_z)/\varphi(\langle\mu\rangle)$.

4. Practice

As an idealizable numerical-analytical procedure, radarclinometry has been completely described at this point. It is even practical in the sense that it has been reduced to an initial value problem rather than one in which all the unknowns must be dealt with simultaneously, and, as a result, a very large matrix inverted. Nevertheless, a number of considerations contrive to make practice confine itself narrowly in comparison to theory as broadly guided by the foregoing sections.

The simplest consideration in this area relates to the mesh fine-ness of integration as optimized in numerical analysis, on the one hand, and the proper application of sampling theory in the digital rendition of an image, on the other. According to the Nyquist criterion, if the digital sampling frequency is equal to or greater than twice the highest sinusoidal frequency in the Fourier transform of a continuous signal, there will be neither a loss of information from, nor an introduction of aliasing errors into, that signal, as represented by the resulting digital file. Economics dictates the use of no higher a sampling frequency than necessary. By comparison, the proper step-size in the independent variables of a system of differential equations to be rendered as corresponding finite-difference equations, is properly one over which considerably less function development can take place. The interval over which solution is required is usually externally imposed. In this case it is the size of an image processed, in *kilometers*. One must first avoid divergence and thereupon seek precision. The higher the precision of arithmetic one is willing to employ the finer the stepping interval one may use and the better will be the solution, in first-order systems at least. But when the driving function of an inhomogeneous equation is not a given, potentially infinitely-precise function, but instead is a record of data in the presence of systematic error and noise, the problem becomes greatly compounded. Bad enough that the factor of at least 10 over the Nyquist frequency, that is desirable for the avoidance of accumulated truncation and linear-extrapolation errors, greatly increases computation time and allocated memory. In fact, the accumulation of true noise in the integration cannot be alleviated by increasing the mesh-fineness. Nor can it be substantially tolerated in an arithmetically non-linear process. Given the signal-to-noise ratio of the radar images that have thus far been available to us, the net result of these considerations is that the highly information-cumulative method of integrating area-wise photoclinometric extrapolations of topographic profiles has been abandoned in favor of the independent line-pair-by-line-pair application of the method of boundary profile formation already discussed. Thus the local-cylindricity

hypothesis pervades the entire topographic file produced rather than merely the boundary profile. The starting value of η for each line is found using the *initial* calculations of $\partial^2 z/\partial y^2$ and $\partial^2 z/\partial x \partial y$ from the preceding line and an equation analogous to the η re-evaluation in Equations (23). One can see quite specifically part of the intolerance to noise of the original theoretical approach in the fact that what is essentially brightness-gradient information is required to determine the sign of $\partial z/\partial y$ according to Equation (9). When the gradient becomes low the sign fluctuation that can set in due to data noise produces fluctuations in $\partial z/\partial x$ in the next line of integration that tends to drive $\partial z/\partial y$ to imaginary values. A practical threshold on the gradient, below which one uses the *preceding* sign of $\partial z/\partial y$ rather than an immediately determined signature is necessary in any event. We may reasonably hope for future radar image quality that will permit the original unprejudiced approach to be used. In the mean time a method which precludes the image-wide propagation of errors is being employed.

When the incorporation of multiple practical expediencies into an already mathematically correct procedure is undertaken, the problem of optimizing the combination may involve far more computation than can be practically funded. One still sees things one would like to try but priorities do not permit. One may also wish to undo a feature incorporated before other changes were made, with the same limitation on action. That may be the nature of the following procedural modification.

In order to avoid enlarging the region of the radar image into which it was necessary to venture on the basis of Equations (10), and to minimize the effects of broadly distributed photometric non-uniformity, an iterative procedure designed to adapt the calibration constant to each line in the enforcement of zero average slope was formulated. Thus the value of z and x at $x' = 0$ are assigned to zero. Each line is integrated twice with revised value of C following each integration. An integral for the correction to C designed to force the value of z at the opposite end of the line to zero can be found based on Newton's method. Specifically acknowledging the dependence of this value of z (at $x' = x = l$) on C, then ideally,

$$z(l, C) = 0.$$

But if not, then determine a correction, ΔC, such that

$$Z(l, C) + \frac{\mathrm{d}z}{\mathrm{d}C} \Delta C = 0.$$

Now

$$z(l, C) = \int_0^l \frac{\partial z}{\partial x} \, \mathrm{d}x$$

carried out at constant y, so that

$$\frac{\mathrm{d}z}{\mathrm{d}C} = \int_0^l \frac{\partial^2 z}{\partial \mu \partial x} \frac{\mathrm{d}\mu}{\mathrm{d}C} \, \mathrm{d}x. \tag{36}$$

In Equation (35), $d\mu/dC = -\varphi(\mu)/C\, d\varphi/d\mu$; and if we assume η is insensitive to C, the mixed partial can be found by differentiating Equation (7);

$$\frac{\partial^2 z}{\partial \mu \partial x} = -\left[1 + \left(\frac{\partial z}{\partial x}\right)^2 + \left(\frac{\partial z}{\partial y}\right)^2\right] \Big/ \left\{\mu(\eta^2 + 1)\frac{\partial z}{\partial x} + e_x \mu^{-1}\left(e_z - e_x \frac{\partial z}{\partial x}\right)\right\}, \tag{37}$$

where all the ingredients of the right hand side are calculated at each point of the integration of topography. The method converges quite rapidly. An iteration is rejected *only* if $|z(l, c)|$ gets larger *and* the number of incidents of imaginary slopes goes up. With the best data currently available, the imaginary-slope incidence rate stands at a third of a percent.

When an entire topographic file has been integrated according to the foregoing scheme, a linear adjustment is made on each line of topography employing the average indications of the data for that line to the effect that its mean slope toward the radar is not zero and its mean height differs from that of its adjacent and preceding line. When an average is a line-average rather than a frame-average it will be denoted by a subscript y. We note that $\langle \partial z/\partial x \rangle_y < 0$ will bias the calibration in the opposite sense from $\langle \partial z/\partial x \rangle_y > 0$ whereas only $\langle |\partial z/\partial y| \rangle_y$ matters for the azimuth component. We therefore form $\langle \partial z/\partial y \rangle_y$ for each line in the original set of integrations as indicative of variation in $\langle z \rangle_y$, notwithstanding the ongoing manipulation of the calibration constant. After all, the choice of $z = 0$ at $x = x' = 0$ was entirely arbitrary and independent of the photoclinometric procedure. Secondly, we form $\langle \partial z/\partial x \rangle_y$ different from zero as an effect due entirely to the variation from nominal calibration and indicative of a proper $z(l) - z(0)$. The line-average of $\partial z/\partial x$ will be much less than its peak value and a first-order calculation attributing all departure in $\langle \mu \rangle_y$ from e_z as due entirely to $\langle \partial z/\partial x \rangle_y \neq 0$ is warranted. Thus

$$\left\langle \frac{\partial z}{\partial x} \right\rangle_y = \tan\left[(\langle b \rangle_y - \langle b \rangle)/e_z \left.\frac{\partial z}{d\mu}\right|_{\mu=\mu_0}\right],$$

$$\langle z \rangle_y = \int_0^y \left(\left\langle \frac{\partial z}{\partial y} \right\rangle_y - \left\langle \frac{\partial z}{\partial y} \right\rangle\right) dy;$$

whereupon

$$x_{\min} = \left(\langle z \rangle_y - \frac{l}{2}\left\langle \frac{\partial z}{\partial x} \right\rangle_y\right) \tan \alpha,$$

$$x_{\max} = l + \left(\langle z \rangle_y - \frac{l}{2}\left\langle \frac{\partial z}{\partial x} \right\rangle_y\right) \tan \alpha,$$

$$\Delta z\,(x_{\min}) = \langle z \rangle_y - \frac{l}{2}\left\langle \frac{\partial z}{\partial x} \right\rangle_y,$$

$$\Delta z\,(x_{\max}) = \langle z \rangle_y - \frac{l}{2}\left\langle \frac{\partial z}{\partial x} \right\rangle_y,$$

The original line of topography is now remapped from the interval $0 \rightarrow l$ to the interval $x_{\min} \rightarrow x_{\max}$. At each of the new positions on the mean datum a Δz is linearly interpolated between the extreme values indicated by the last two members of equation set (38) and added to the value of z which was mapped from the original integration file.

The foregoing procedure enables one to develop topography in correspondence with an entire image. In retrospect, it seems superior to retain the original frame-wide calibration and operate photoclinometrically on a sub-frame of the image. Thus the values of $\partial z/\partial y$ and $\partial^2 z/\partial y^2$ computed at the beginning of each line determine an integration step to the starting value of z when beginning integration on the subsequent line, and not merely a new starting value of η. Thereby, also, one must reposition the correspondence with the image, since $x' = 0$ no longer corresponds to $x = 0$, as indeed, in general, it should not.

A few additional minor practicalities are worthy of mention. Solution of Equation (22) by the quadratic formula occasionally comes perilously close to zero-over-zero. The first order solution, $\partial z/\partial x = (e_z - \mu)/e_x$ should be used when a value check indicates it is applicable. Closeness to division by zero also must be checked in the η iterations, and the step avoided if indicated. A check should also be run on the closeness of the argument of the square-root to zero, whether positive or negative, assuming a reasonable value for numerical noise, in solving Equation (22). Under appropriate conditions the plane of constant η is then taken as tangent to the cone of constant μ. Given all these considerations, it will still happen occasionally that Equation (22) yields a distinctly complex rather than a real slope. When this happens it is time to admit that the integration has accumulated sufficient noise and error that it is currently absurd. It must be either that current erroneous variations in μ or the wayward development of η are responsible for this. When this occurs, no integration step is taken and η is reset to zero. The last real value of $\partial z/\partial x$ is stored. The attempted integration proceeds until a real value of $\partial z/\partial x$ is again found. The arithmetic mean of this value and the stored value is adopted and used to integrate over the gap that has developed. No second order terms are allowed in the stepping when this occurs.

Since errors of a significant size do appear in photoclinometry and are 1-dimensionally concentrated due to quasi-independent line-by-line integration techniques, one wishes to develop a counterpart to the adjustment theory which serves photogrammetry. Though mathematically quite different, it should be based on the same criteria that such errors as are already present should be more equitably distributed and if not reduced, at least not increased; and such adjustment as is employed should not lead to a loss of real information.

Let's begin with the assumption that sampling theory has been properly observed in determining the original digital image. Then the spatial spectrum of that image will be fully contained below a Fourier frequency of ½ the digital sampling frequency. The only difference between the original continuous-image spectrum and the spectrum of the digitized image is that the latter consists of the scaled original plus its

scaled reproductions, shifted from a center at zero to centers at the sampling frequency and its harmonics. The Nyquist criterion simply requires that the assemblage of shifted Fourier transforms contains no overlap.

A function and all its derivatives have Fourier transforms whose non-zero extent are confined to the same spatial frequency interval; and if photoclinometry were a mathematically linear process we could conclude straight-away that the topography must have a Fourier transform confined to the same frequency interval as that of the image. We may appeal to the convolution theorem of Fourier analysis to conclude that the highest power to which $\mu(x, y)$ or its gradient components are raised in the determination of photoclinometric topography is equal to the ratio of the confining spatial frequency range for the Fourier transform of the topography to that for the Fourier transform of $\mu(x, y)$. This conclusion is valid for fractional as well as multiple exponents. What are its implications?

Let us rewrite Equation (7) in a more immediately useful form

$$e_z^2 - 2e_z e_x \frac{\partial z}{\partial x} + e_x^2 \left(\frac{\partial z}{\partial x}\right)^2 = [\mu(x, y)]^2 \left[1 + \frac{\partial z}{\partial x}\right)^2 + \left(\frac{\partial z}{\partial y}\right)^2 \Bigg]. \tag{40}$$

This equation is the most general of those used and contains implicity the consequences of all the rest for our immediate goals. Let's refer to the Fourier transform of $z(x, y)$ as $\zeta(\omega_x, \omega_y)$ (so the Fourier transform of $\partial z/\partial x$ is $\imath\omega_x\zeta(\omega_x, \omega_y)$ and the Fourier transform of μ as $U(\omega_x, \omega_y)$. We will use the enlarged line-level asterisk to denote convolution. Taking the Fourier transform of both sides of Equation (39), we find that

$$\begin{aligned} &e_z^2\delta(\omega_x)\delta(\omega_y) - 2\imath e_z e_x \omega_x\zeta(\omega_x, \omega_y) - e_x^2[\omega_x\zeta(\omega_x, \omega_y)] * [\omega_x\zeta(\omega_x, \omega_y)] = \\ &= U(\omega_x, \omega_y) * U(\omega_x, \omega_y) * \{\delta(\omega_x)\delta(\omega_y) - [\omega_x\zeta(\omega_x, \omega_y)] * [\omega_x\zeta(\omega_x, \omega_y)] - \\ &- [\omega_y\zeta(\omega_x, \omega_y)] * [\omega_y\zeta(\omega_x, \omega_y)]\}. \end{aligned} \tag{41}$$

Equation (40) is really of interest to us only because it requires the spatial frequency bandwiths of both sides to accomodate one another. The bandwidths of the Dirac delta-functions shown are zero and we dismiss them immediately. When we convolve $\omega_x\zeta$ with itself, the result has double the bandwidth of $\omega_x\zeta$. Therefore, the left-hand-side of Equation (40) has a bandwidth double that of ζ, or double that of the spatial spectrum of $z(x, y)$ itself. The greatest number of convolutions on the right-hand-side of (40) is four, and it seems to demand a bandwidth equal to the sum of twice the bandwidth of ζ plus twice the bandwidth of U. This may seem contradictory until we remember that the functions in the equation are not independent of one another. Let's look at Equation (40) more closely. On the face of it, there is *no way* the left-hand-side can be non-zero for values of ω_x or ω_y greater than twice the cut-off frequencies in the topographic spectrum. Similarly, there is *no way* the right-hand-side can be non-zero for spatial frequencies outside the larger range mentioned above. Evidently, then, for spatial frequencies that are intermediate – outside the smaller

band but inside the larger band – there *is* a way for the right-hand-side to be zero that relies on the special relations between ζ and U, so that the equation can be satisfied. For spatial frequencies inside the smaller band, then, we have no grounds for forcing both sides of Equation (40) to zero. On the other hand, the first term on the right-hand-side of Equation (40) is $U * U$, whose bandwidth is, independently of ζ, twice the bandwidth of U. Hence, twice the bandwidth of ζ equals twice the bandwidth of U, or simply, the spatial frequency cut-offs are the same in the derived topography as for the image.

Based on the foregoing conclusion, any extension of the Fourier transform of our derived topography to frequencies in excess of one-half the digital sampling frequency for the original image is not real topographic information and may be justifiably removed. The spectra of the original image and the final topography should both *smoothly apodize* to zero at the same spatial frequency cut-off.

The physical formation of an image of an object by a lens passing incoherent light is one in which the apodizing function acting on the Fourier transform of the object to produce the Fourier transform of the image is almost linear. To the extent that radar does not emulate this practice it is thoroughly uncooperative! It is always helpful, when practical, to re-apodize SAR images before applying radarclinometry.

If we let $\Upsilon(\omega_x, \omega_y)$ be of form $\Upsilon(\omega)$, with $\omega = (\omega_x^2 + \omega_y^2)^{1/2}$, and which equals 1 when its argument is zero and proceeds linearly to zero when its spatial frequency argument equals ½ the sampling frequency, then an optimum procedure might be to take the Fourier transform of the topography and then take the inverse Fourier transform of $\zeta(\omega_x, \omega_y)\Upsilon(\omega_x, \omega_y)$ as a final adopted topography. Unfortunately, two-dimensional Fourier transforms are not practical for most of us, so a compromise is desired. Remembering that $z(x, y)$ was produced as a set of quasi-independent tabulated indefinite integrals in the x direction, we may well expect that the spurious high-frequency Fourier components should be concentrated in ω_y relative to ω_x. Furthermore, the accumulation of spurious slopes in the integration in the x direction will introduce spurious low frequencies as well as spurious high frequencies in ω_x, whereas almost exclusively high frequencies are introduced in ω_y. A reasonable approach is therefore to rotate the topography 90° so that a read-in line to be operated on is now a sequence delineated by y rather than x, and do a one-dimensional re-apodization on a line-by-line basis. Instead of simply removing all artifactual striping in x, such an approach will tend also to introduce such striping in the dimension perpendicular to x. However, it should be greatly subdued. This is the approach that has been adopted.

5. Contingency-Processing

The procedures outlined in the foregoing sections, whether optimal or otherwise, may be characterized as general. One would apply all of them, in one form or another, in order to maximize the extraction of topographic information from the radar data. By contingency-processing we shall mean those operations which are

known to invade the information spectrum to at least some degree, but whose compromising effects are deemed to be offset by the obvious alleviation of problems created by random noise and systematic error in the data. I have felt obliged to create one such algorithm, which applies in the following way.

The tendency toward artifactual 'striping' is alleviated by the one-dimensional Fourier filtering of the entire image, as described in the previous section, at no expense to the actual information. A technique is necessary in order to deal with artifactual 'banding', i.e., the presence of this form of noise at spatial frequencies well below the Nyquist cut-off. The approach that has been developed for dealing with this problem is based on the assumption that it exists primarily as the result of error in the adjustment of the mean-height and mean-slope of each range-line integration. Using this assumption we refrain from adjusting *directly* the amplitudes of the Fourier components of the topographic array, and instead operate on the spatial spectra of the linearization parameters. The process is carried out in four steps. (1) Four one-dimensional arrays are created by the least-square fitting of straight lines to each topographic profile in range, as a member of a set delineated in azimuth, and each topographic profile in azimuth, as a member of a set delineated in range. (2) The next and all remaining steps are applied to the constants and the linear coefficients independently. The power-spectra as well as the complex Fourier transforms are taken of, say, the constants, now conceived as two functions, one of azimuth and the other of range. (3) Beginning at a spatial frequency that is specified on the basis of a visual appraisal of the topographic file portrayed as an image, the Fourier transform of linearization-constant-versus-azimuth is normalized in amplitude so that, maintaining continuity at the beginning wavelength, the corresponding power spectrum is brought into constant ratio with the power spectrum of linearization-constant-versus-range at all higher spatial frequencies. (4) The inverse transform is taken of the result and the revised constant-versus-azimuth is used together with a similarly revised linear-coefficient-versus-azimuth to readjust both the heights and mean-datum-placements of each topographic profile down range.

It is difficult to justify the above process on other than pragmatic grounds. It is certainly reasonable to suppose that when artifactual banding is parallel to ground-range, the run of linearization constants with azimuth will show such banding, whereas the orthogonally fitted run of linearization constants with ground-range will smooth out such effects. We thus hope to alleviate the effect on the topographic file as a whole by requiring the first run to emulate the second insofar as its Fourier amplitudes above a certain frequency are concerned, while preserving intact all the relative phases. It can further be stated that this procedure will not introduce any systematic errors of its own if the assumption be granted that the two-dimensional autocorrelation function of the topography is isotropic in all but the broadest scale of its variations. Other methods of dealing with the problem of poor photometric leverage on azimuthal slope components will be welcomed in future investigations, however they have yet to be conceived.

6. Results of Application

The first application of radarclinometry to real data was made on a digital radar image of the Algodones sand dune field near Yuma, Arizona, obtained by the SEASAT SAR. Except for the setting of an automatic-gain-control the image signal is available in a form proportional to the reflected electric vector amplitude and is in this sense photometrically calibrated. The back-scattering function employed in the data reduction was taken from the 'Radar Cross-section Handbook' (Ruck *et al.*, 1970) for dry sand. There is also an obvious sense in which the terrain is homogeneous, naively assumable to benefit our prospects of success. Although the main program successfully produced a result, it appeared to have little genuine topographic significance. A worse choice would have been difficult to find, and this appears to have been the case for a composite of reasons:

(1) The extreme depression angle of 72° greatly increased the likelihood of a vanishing Jacobian and also made horizontal pixel-shifting extremely sensitive to photometric error.

(2) The digital sampling interval appeared not to obey the Nyquist criterion. The average dune dimension did not greatly exceed the sampling interval. When the image was re-apodized for the alleviation of this problem and the speckle problem, only the broader topographic variations emerged, which the automatic-gain-control rendered meaningless.

(3) Sand is a specular reflector at radar wavelengths. The mimicry of diffuse reflection occurs only because the resolution element of the image is large enough to contain a statistical aggregate of optical facets, somewhat randomly aligned. But a resolution element 20 meters across does not present a satisfyingly large statistical sample of optical facets. The possibility of the reflection being dominated by a single facet aligned almost normally to the radar propagation vector also contributes to a situation wherein the terrain is actually not very homogeneous in radar back-scattering function. Operating on the steep shoulder of the radar back-scattering function compounds this problem.

(4) The state of the sand has some bearing on the statistical distribution of optical facets. A back-scattering curve obtained by working off the vertical on flat sand is not identifiable with one obtained by varying the tilt of the sand. Leeward and windward dune faces can be expected to possess different radar photometric functions. Thus the diffuse reflectivity of the surface can be expected to be inhomogeneous in both sporadic and systematic ways. The findings of Blom and Elachi (1981) corroborate this view.

After the frustations of the preceding effort, it was decided to concentrate work on low depression-angle SLAR frames. The one drawback to this choice was the total unavailability of photometric calibrations. The assumed calibration was thus completely heuristic. Only a qualitative test is thus encountered. Inasmuch as the method has been designed to approach the metric integrity of photogrammetry as closely as possible, no small concession has been made in doing this. Although low depression

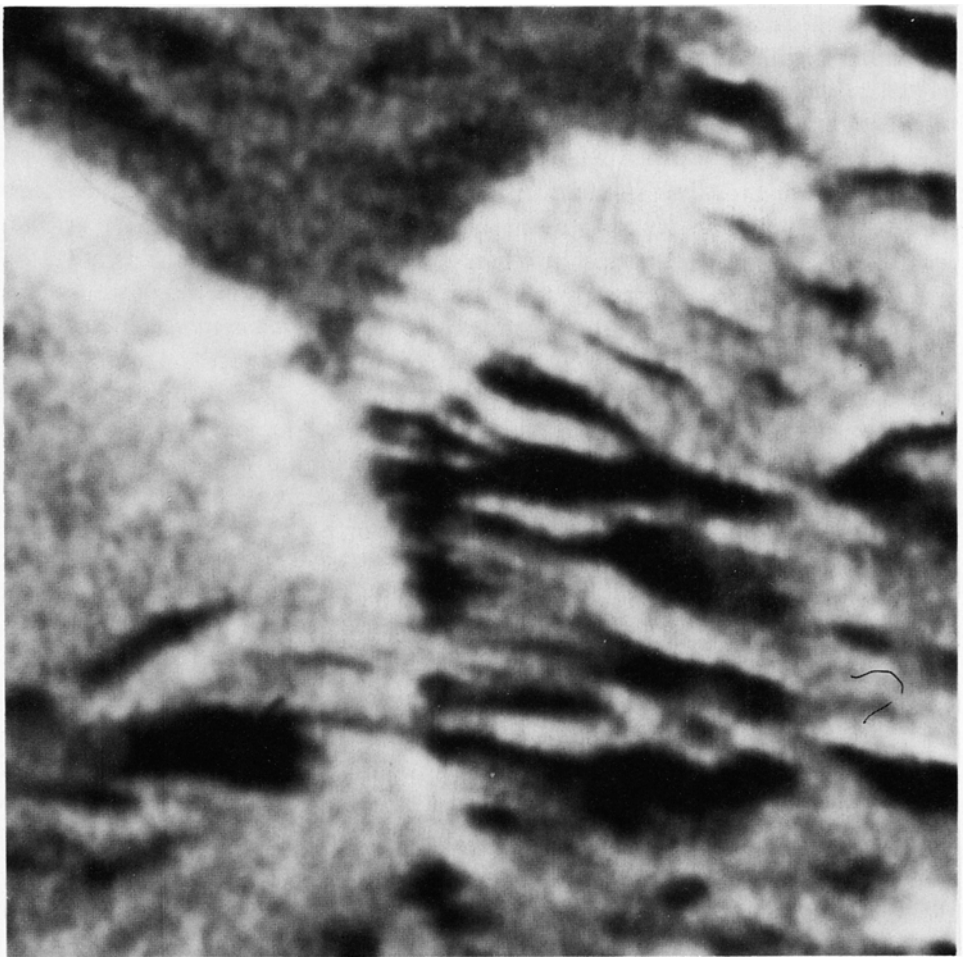

Fig. 2. Motorola radar image of Crazy Jug Point in Grand Canyon National Park.

angles introduce radar shadows, the processing problem thus presented is a mild one; the envelope of radar-ray distribution assumes the role of the terrain.

The form in which the SLAR data was made available was that of second-generation positive photographic transparency. The source of data was the Motorola Corporation. These film strips are archival at the U.S. Geological Survey in Flagstaff, Arizona, so a negative transparency suitable for digitizing at the USGS Flagstaff Image Processing Facility was generated by the photographic laboratory of the Flagstaff Field Center. An Optronics output of the re-apodized digital radar image is shown in Figure 2. The region investigated is Crazy Jug Point in the Grand Canyon of the Colorado River. North is approximately at the top and the frame is about 15 kilometers wide. Digitally, the frame is 630 lines by 630 samples. This is the frame which was processed with the 0.3% slope-abort-incidence-rate mentioned

earlier. The Radar Cross-Section Handbook curve for broken desert was used and the photometric calibration curve was obtained by assuming that the digital values of optical density, after subtraction of the darkest radar shadow, were proportional to the radar reflected specific intensity. This is equivalent to assuming that one photon in the final printing renders one photographic grain stably developable, and that the accumulated cross-section density of developable grains is much less than one. Of course the final photon flux density is assumed proportional to the original radar specific intensity. These assumptions are demonstrably unrealistic, but they are as realistic as any available alternatives, and more easily incorporated.

The main radarclinometry program required 20 hours of computation time on the DEC PDP11/45 of the U.S.G.S. Flagstaff computer, using the DOS BATCH operating system. The subsequent spatial frequency filtering and amplitude-normalization programs for height/tilt readjustment made use of a Floating Point Systems Array Processor and required only a few minutes.

Because no photometric calibration exists, we have elected not to present a direct comparison of a topographic contour-mapped version of our digital topographic file with the corresponding region of topographic map N3600–W11145/28 × 60 compiled by the U.S. Geological Survey and the U.S. Coast and Geodetic Survey, though that will be a result of future research, if successful. It would be scientifically ludicrous to present a test of the fortuitousness with which a photometric calibration had been randomly achieved. A method of testing is needed which separates this effect from the qualitative appreciation of the relative placement of heights of promontories and depressions. Accordingly, the following procedure was carried through. A corresponding digital topographic file was hand-punched from the USGS/USCGS map. Registration of corners was eye-estimated without preserving orthogonality. A crude attempt was made to match the resolution of the radarclinometric file. Both this topographic file (photogrammetric) and the radarclinometric topographic file were processed to produce shaded relief maps in stereo-optical pairs. The shaded-relief files were generated by placing an artificial sun 30 degrees above the north horizon (opposite the original radar) and generating surface brightness according to Lambert scattering and the incidence angles implied by the topographic file, using the algorithm originally devised by Batson *et al.* (1975). The synthetic stereo-mate was generated by shifting pixels in the shaded relief file along the East–West line proportional to the values of z in the topographic file (Batson *et al.* 1976). The result is presented in Figure 3, which speaks for itself.

7. Future Prospects

Several realignments of effort have already been discussed, but the most urgent consideration is the reduction of computation time. It is the principle reason why a wider variety of processing and a larger volume of products have not been reported in this paper. A refined method for re-apodizing the original image can lead to discarding the calibration-iteration procedure and the elimination of some averaging techniques

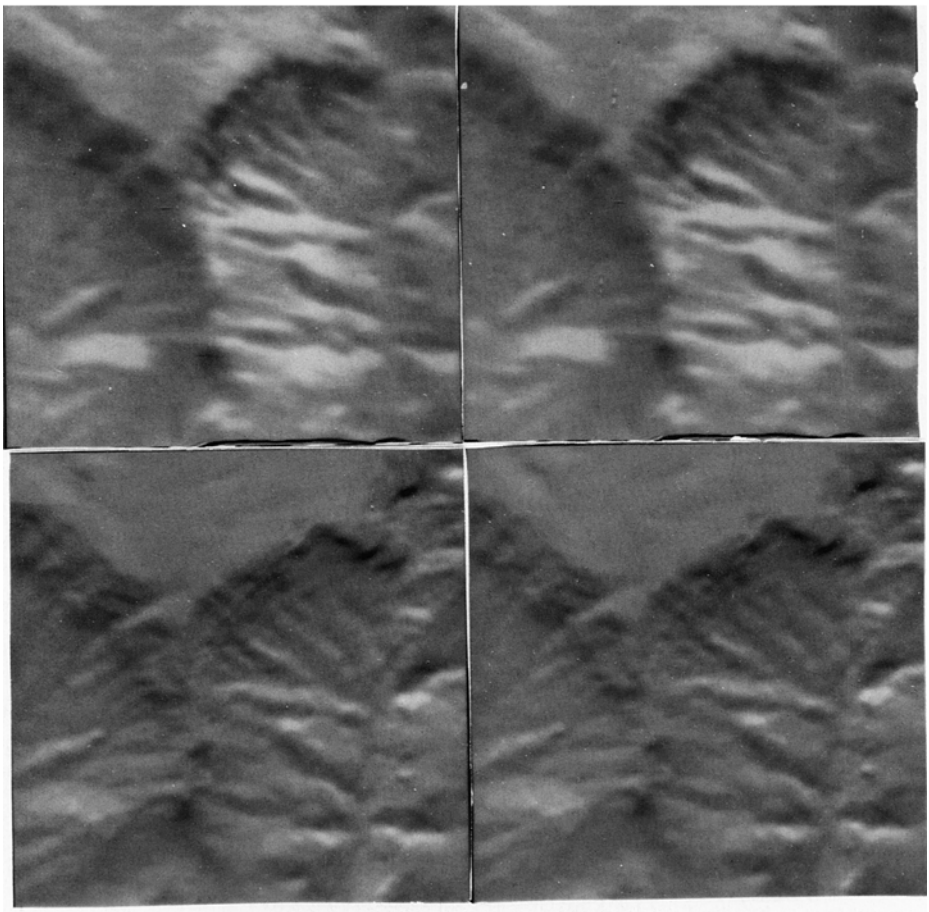

Fig. 3. Two stereograms in shaded-relief images of Crazy Jug Point. The upper stereo-pair was generated from a radarclinometric topographic file. The lower stereo-pair was generated from a photogrammetric topographic file. The effective sun-angles of the shaded relief renditions are not the same because of unknown relative tilt in the two mean datums.

that are costly in terms of disk-file manipulation. We can reasonably hope to cut run-time by a factor of four. If a number of fail-safe-motivated logical branchings can also be eliminated, use may be made of the Array Processor in the main program to achieve an additional factor of two or even higher. From this point on, only a trial-and-error evolution of the method can be foreseen, and improvement will require considerable effort.

The poor photometric leverage on cross-slopes remains a serious problem and some additional creative ideas for dealing with it that involve a minimal invention of science-fiction would be welcome.

Two obvious recommendations come out of this study. (1) The photometric calibration of radar images is *very important*. It should receive far more attention

from the developers of imaging radars and their signal reduction systems than has been the case up to now. Upgrading the signal-to-noise ratio of a pixel, and look-smoothing of speckle, also deserve higher priority. A radar image is no longer simply the object of a subjective Gestalt formation, but an important quantitative array. (2) Almost all the depression angles that have been used are either too large or too small from a radarclinometric viewpoint, though too small is definitely preferable. Forty-five degrees is about optimum. Only the Space Shuttle radar (SIR-A and SIR-B experiments) comes close to this, at 50 degrees. I look forward to working with it in the future.

Among other related future research efforts are field investigations of the back-scattering versus incidence angle for a wider variety of terrain types and under a variety of seasonal variations. Included in this would be measurements of heterogeneity within a given terrain type under a given seasonal condition. The present method also offers possibilities where no others may be forthcoming for the determination of file-scale Cytherean topography from radar images to be obtained by the Venus Radar Mapper mission later in the decade. I am also looking into the application of the local-cylindricity hypothesis to traditional sun-observer photoclinometry, and alternative integrability-assumptions such as local sphericity, which might be of a non-default character and occasionally triggered into processing on the basis of criteria related to higher derivatives of the image.

In summary, radarclinometry has proven to hold significant promise as a method of determining topography under conditions which make it a useful alternative. The extension of the present work in future efforts is concretely self suggesting in a variety of ways.

Acknowledgements

It is a pleasure to thank Eric Eliason, Pat S. Chavez, Jr., and Alex Acosta for a variety of computational and logistic services. Thanks also go to Larry Soderblom and Henry Moore for reviewing an earlier version of this manuscript. This work was supported by the Geologic Division, U.S. Geological Survey, Dept. of the Interior, and Planetary Geology Programs Office, National Aeronautics and Space Administration.

References

Batson, R. M., Edwards, K., and Eliason, E. M.: 1975, *J. Res. U.S. Geol. Surv.* **3**, 401.

Batson, R. M., Edwards, K., and Eliason, E. M.: 1975, *Photogram. Engineer. and Remote Sens.* **42**, 1279.

Birrer, I. J., Bracalente, E. M., Dome, G. J., Sweet, J., and Berthold, G.: 1982, *IEEE Trans. Geoscience Remote Sens.* **GE-20**, 11.

Blom, R. and Elachi, C.: 1981, *J. Geophys. Res.* **86**, 3061.

Diggelen, J. van: 1951, *Bull. Astron. Inst. Netherlands* **11**, 283.

Eliason, P. T., Soderblom, L. A., and Chavez, P. S. Jr.: 1981, *Photogram. Engineer. Remote Sens.* **48**, 1571.

Lambiotte, J. J. and Taylor, G. R.: 1967, Conference on the use of Space Systems for Planetary Geology and Geophysics, May 25–27, 1967, Boston, Massachusetts.
Minnaert, M.: 1941, *Astrophys. J.* **93**, 403.
Rindfleisch, T.: 1966, *Photogram. Engineer.* **32**, 262.
Ruck, G. T., Barrick, D. E., Stuart, W. D., and Krichbaum, C. K.: 1970, *The Radar Cross-Section Handbook*. Plenum Press, New York, London, 453 pp.
Schaber, G. G., Berlin, G. L., and Brown, W. E., Jr.: 1976, *Geol. Soc. Am. Bull.* **87**, 29.
Watson, K.: 1968, *U.S. Geol. Surv. Prof. Paper* **599B**, 10 p.
Wildey, R. L.: 1974, *Nature* **249**, 132.
Wildey, R. L.: 1975, *Icarus* **25**, 613.
Wildey, R. L.: 1978, *Science* **200**, 1265.